



# High speed flow visualization of a closed loop pulsating heat pipe

J.L. Xu <sup>a,\*</sup>, Y.X. Li <sup>a,b</sup>, T.N. Wong <sup>c</sup>

<sup>a</sup> *Guangzhou Institute of Energy Conversion, Chinese Academy of Sciences, Nengyuan Road, Wushan 510640, PR China*

<sup>b</sup> *Graduate School of Chinese Academy of Science, Beijing 100039, PR China*

<sup>c</sup> *School of Mechanical and Production Engineering, Nanyang Technology University, Nanyang Avenue 639798, Singapore*

Received 8 April 2004; received in revised form 7 February 2005

## Abstract

We provide the high speed flow visualization results for the closed loop pulsating heat pipes (PHPs). It is identified that there exists the bulk circulation flow which lasts longer and the local flow direction switch flow. The bubble displacements and velocities do display the sine oscillation waves but the local oscillation waves were superimposed with short periods and small oscillation amplitudes. Distinct with the methanol PHP, the water PHP has quasi-rectangular shape for the bubble displacements, behaving the periodic stationary-fast movement characteristics. Dispersed bubbles, vapor plugs and the transition flow patterns from the dispersed bubbles to the vapor plugs are the major flow patterns in PHP. Long vapor plugs are only observed for the methanol PHP, not observed in the water PHP, due to the vapor plug deformation and breakup mechanism, which was analyzed in the present paper. Bubble sizes have quasi-fixed distributions versus time over the entire PHP, but have unsymmetry distributions among various tubes. The complicated combined effects of bubble nucleation, coalescence and condensation are responsible for the oscillation flow in PHP. © 2005 Elsevier Ltd. All rights reserved.

## 1. Introduction

Pulsating heat pipe (PHP), first proposed by Akachi [1], is considered as a possible thermal management solution for the high heat flux electronic cooling. Due to the fast development of the high heat flux electronic component in the semiconductor industry in recent years, PHP has been received great attention, possibly due to the novel working principle and the low fabrication cost using the copper capillary tubes. The working fluid will arrange in slug-train units in the PHP due to the surface tension effect. Heat is transported from the

evaporation to the condensation zones by means of local axial oscillations and phase change heat transfer in the working fluid. Circulation of the working fluid is possible for the closed loop PHP and this effect further enhances the capability for the working fluid to transport heat from the evaporation to the condensation zone.

Gi et al. [2] studied an “O” shaped PHP as it is applied to a cooling of CPU chip. Their results showed that the CPU chip temperature can be up to 90 °C with the heating power less than 40 W, which is the maximum limit for the safe use of the CPU chip. Wong et al. [3] proposed a theoretical model in terms of a Lagrangian approach in which the flow was modeled at adiabatic conditions for the whole PHP. A sudden pressure pulse was applied to simulate the heat input over a vapor plug.

\* Corresponding author. Tel./fax: +86 20 87057656.  
E-mail address: [xujl@ms.giec.ac.cn](mailto:xujl@ms.giec.ac.cn) (J.L. Xu).

**Nomenclature**

|                      |   |                        |  |
|----------------------|---|------------------------|--|
| $Bo$                 | Bond number   | $R_i$                  | inside radius of the capillary tube, m                               |
| $Bo^* = q/(Gh_{fg})$ | boiling number  | $t$                    | time, s  |
| $Ca$                 | capillary number  | $U$                    | velocity, m/s  |
| $D$                  | inside diameter of the capillary tube, m                    | $We = LG^2/\rho\sigma$ | Web number   |
| $Eo$                 | similar to $Bo$ , but scaled as any physical related length | $z$                    | axial coordinate attached on the centerline of the capillary tube, m |
| $ET$                 | time lasts for the flow direction switch process, s         | $\delta$               | non-dimensional liquid film thickness                                |
| $G$                  | mass flux, $\text{kg}/\text{m}^2 \text{ s}$                 | $\Delta t$             | time step for each successive image, s                               |
| $g$                  | gravity, $\text{m}/\text{s}^2$                              | $\Delta T$             | time needed for a full process, s                                    |
| $h_{fg}$             | evaporation of heat, $\text{J}/\text{kg}$                   | $\mu$                  | dynamic viscosity, $\text{kg}/\text{ms}$                             |
| $h$                  | liquid film thickness, m                                    | $\rho_f, \rho_g$       | liquid and vapor density, $\text{kg}/\text{m}^3$                     |
| $L$                  | length of bubble, or any other physical related length, m   | $\sigma$               | surface tension force, N   |
| $p$                  | pressure, Pa  | $\Delta p$             | pressure difference, Pa  |
| $q$                  | heat flux, $\text{W}/\text{m}^2$                            | $\Gamma$               | non-dimensional radius ratio   |
| $R_1, R_2$           | principal radius of the curvatures, m                       | <i>Subscripts</i>      |  |
| $R_b$                | centerline curvature of the inverted U bend, m              | f                      | liquid phase   |
|                      |   | v                      | vapor phase  |

They could show the pressure and velocity oscillations versus time for the selected vapor plug. Shafii et al. [4,5] performed the numerical modeling of PHP with multiple liquid and vapor plugs using the constant wall temperature condition. They illustrated that the gravity force has an insignificant effect on the performance. They also demonstrated that the major heat transfer mechanism is due to the sensible heat and the PHP does not work at high fill ratios such as higher than 90%. Tong et al. [6] performed the flow visualization for the closed loop PHP. It was observed that during the start-up process the working fluid oscillates with large amplitude. The working fluid circulates for the steady oscillation state. Charoensawan et al. [7,8] performed a wide range of experimental studies providing vital information on the parameter dependence of their performance. The characterization parameters have been done for the variation of the internal diameter, number of turns and inclination angle. Their results strongly indicate the gravity and number of turns effects on the thermal performance. In addition to these, semi-empirical correlations were given.

In our previous paper [9], the PHP heat sink was fabricated using the copper capillary tube with the heat dissipated to the environment by the air natural convection. Temperature (thermal) oscillations at the outer wall surface relating to the vapor plug and liquid slug periodically flushing the inside wall surface were recorded by a high speed data acquisition system. The cycle period of the temperature oscillating is much longer for water PHP than those of PHPs with FC-72 and

ethanol as working fluids. It is concluded that these peculiar phenomena are related to the larger latent heat of evaporation and surface tension for water. The unlooped PHP is not helpful for the fluid circulation and does not work. The optimal fill ratio is suggested to be 0.7 for all the three working fluids of FC-72, ethanol and water.

The above literature survey shows that most of the previous work focus on the thermal performance evaluation and simple flow visualization. The present paper provides detailed high speed flow visualizations and is organized as follows. Section 2 describes the experimental setup. Section 3 describes the oscillation flows based on the present experimental findings, including two subsections, one is the flow direction, the other is the bubble velocities. Section 4 identifies the flow patterns in the closed loop PHP, separating into two subsections, one is the flow patterns and the other is the physical explanation of the vapor plug deformation and breakup. The major conclusions are summarized in Section 5.

## 2. Experimental setup

Fig. 1a illustrates the experimental setup, consisting of the PHP assembly, the power supply unit, and the high speed camera. The PHP assembly was made of high quality glass capillary tube with the outside diameter of 6.0 mm with the wall thickness of 2.0 mm. Thus the inside diameter of the capillary tube is 2.0 mm. The bending radius of the U bend in the evaporator section and

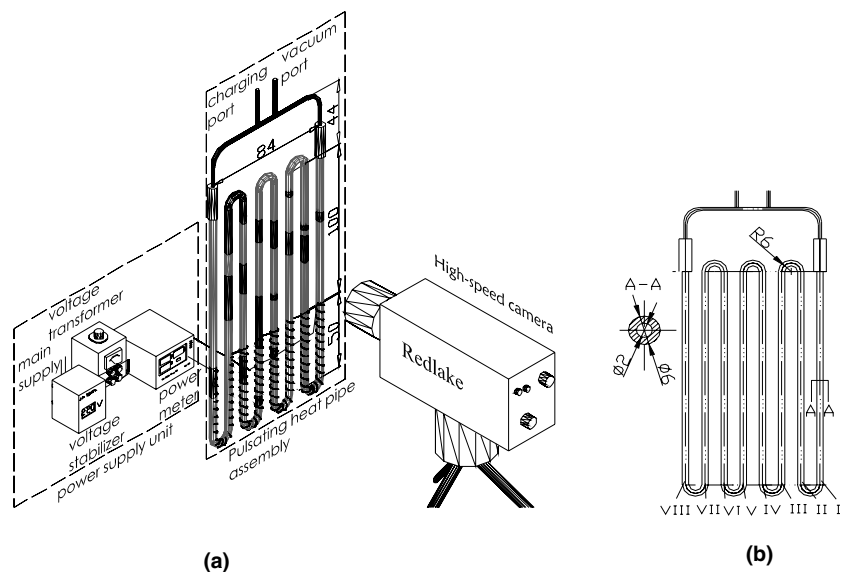


Fig. 1. Experiment setup for the high speed flow visualization of the closed loop PHP.

the inverted U bend in the condensation section is 6.0 mm, forming eight snake-shaped PHP structure. The total height of the PHP is 200 mm with the total width of 90 mm. The height of the evaporator section is 56 mm while the condensation section has the height of 144 mm. The top horizontal copper capillary tube with the vacuum and charging ports arranged connects the glass capillary tube by two tube adaptors. Such piece of hardware can sustain 4 bar pressure without any leakage for eight hours. In the evaporator section, the thermal load was provided by Ni–Cr thermic wire with a diameter of 0.4 mm ( $12 \Omega/\text{m}$ ) which was wrapped at intervals of 1.5 mm on the outer wall surface of the PHP. In order to minimize the heat dissipated to the environment in the evaporator section, the high quality thermal insulation material was wrapped. Because the evaporator section is well heat insulated, the small quantity of heat loss to the environment is difficult to be estimated because PHP is a closed system. The heat received in the evaporator section is nearly totally dissipated to the condensation section, thus the steady oscillation state could be sustained. The air environment temperature is set to be  $24^\circ\text{C}$  which is controlled by the air condition system. The PHP assembly was vertically positioned.

We use the bare glass capillary tube in the condensation section thus the high speed flow visualization could be performed. Due to the small heat transfer coefficient on the outer wall surface, the length of the condensation section is nearly two times of the evaporator section. We use four U-turns of the capillary tube forming eight capillary tubes, thus the oscillation flow could be fully developed inside the PHP system. We use the inside

diameter of 2.00 mm of the capillary tube because such size can satisfy the minimum size requirement to form the slug-train units. Fig. 1b shows the schematic diagram of the PHP, in which the eight capillary tubes are identified as I, II, III, IV, V, VI, VII, VIII from right to left.

The vacuum and charging procedures were performed using a special facility fabricated in our laboratory. The PHP was baked at  $100^\circ\text{C}$ , evacuated to a pressure of  $7.5 \times 10^{-4}$  Torr for eight hours, and then isolated from the vacuum system by seal. The PHP is then filled with the working fluid and sealed. Two working fluids, methanol and deionized water were used in the present study. The nucleation boiling process highly depends on the purity and the dissolved air concentration of the liquid. Methanol has the highest purity and the air dissolved in the liquid can be neglected. The deionized water is heated up to  $90^\circ\text{C}$  and filtered through a  $2 \mu\text{m}$  filter before it is charged into the PHP system. The final net liquid charged in the PHP was the weight difference before and after the PHP was charged with liquid. Such weight measurement was performed by an electronic balance with the uncertainty of 0.01 g. The fill ratio was defined as the total liquid volume divided by the total inside volume. In terms of our previous study (Zhang et al. [9]), the fill ratio of 70% is identified as the optimal value, thus it is used in the present paper. The fill ratios have the uncertainty less than 1.0%.

The power supply unit includes a voltage stabilizer, a voltage transformer, and a powermeter. By adjusting the voltage transformer, one can obtain a stable voltage output in the range of 2–220 V, producing the heating power in the range of 1–100 W. The powermeter

measures the voltage, current and power simultaneously supplied on the evaporator section with the uncertainty of 0.5%.

We present the experimental results at two heating powers of 10.0 W and 30.0 W. There are some differences on the thermal performance and the bubble dynamics at the two heating power extremes. For instance, PHP has less dispersed bubbles at lower heating powers than that at high heating powers. Besides, PHP approaches quasi-sine function wave for the bubble displacements and velocities. However, the complicated local flow direction switch process is superimposed on the bubble velocity curve at the higher heating powers.

The high speed camera is HG-100 K (Redlake Inc., USA). It uses the advanced 1.7 M CMOS sensor, which has the recording rates up to 10,000 frames/s, with the sensitivity of  $1504 \times 1128$  pixels. Based on the present bubble velocity range, the recording rate was selected as 125 frames/s. Using this image sampling rate, the PHP can be continuously viewed for the total time up to 21 s, covering several full oscillating cycles. When the high speed camera is operating, a very powerful light source is turned on to form clear images. The dynamic images can be shown in the PC screen and stored in the PC memory for future process. The time step for each continuous image is 0.008 s corresponding to the recording rate of 125 frames/s. The successively images were processed using the commercial software of Photo-shop 6.

The minimum bubble size that can be detected could be estimated as the overall width of the PHP over the horizontal pixel, leading to  $84 \text{ mm}/1128$  (nearly  $80 \mu\text{m}$ ). Similarly, the bubble length measurements also have the uncertainty of  $80 \mu\text{m}$ . Because the bubble velocities varied from zero to the maximum values periodically, the uncertainties of the bubble velocities depend on the velocity itself. The present measurements show that the maximum bubble velocities are in the order of  $100 \text{ mm/s}$ . For the bubble velocity of  $1.0 \text{ mm/s}$ , the bubble velocities have the largest uncertainties of 10%. Higher bubble velocities such as  $100 \text{ mm/s}$  result in the smaller uncertainties of 0.1%.

### 3. PHP oscillation behavior

#### 3.1. Pulsating flow directions in PHP

Understanding the start-up and steady oscillation flows in PHP are helpful to identify the PHP oscillation behaviors. The start up flow behavior was experimental examined by Tong et al. [6]. Fig. 2 illustrates four vertical capillary tubes for a closed loop PHP, marked as tube 1, 2, 3 and 4. An initial charge of the working fluid inside the PHP results in the randomly distributed vapor plug trains. When a uniform heat flux is applied on the

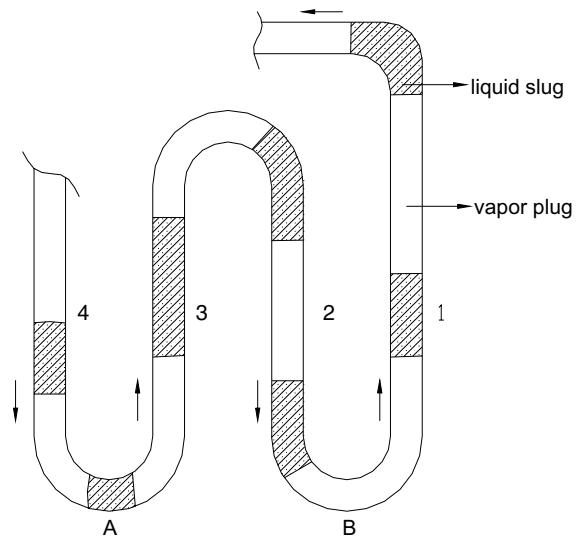


Fig. 2. Schematic diagram showing the PHP working principle.

evaporator section, pressures in each capillary tubes are increased by the bubble nucleation, coalescence and condensation process at different increasing rates, due to the non-uniform distributed vapor plug trains inside. For instance, assuming pressure in point A is higher than that in point B, flow can be initiated as the flow direction as the array marked in Fig. 2. The vapor plug trains across the horizontal tube may be partially condensed thus the left tube receives the downward flow direction. However, after a short time elapsed, the fluid movement as shown in Fig. 2 can substantially change the vapor plug distributions, resulting in the inverse pressure balance between points A and B, leading to an inverse flow direction established. The pulsating flow is maintained inside PHP thus heat received in the evaporator section is transferred to the condensation section.

It is identified in the present paper that once the steady oscillation flow is established there exist the bulk circulation flow and the local flow direction switch flow in a full cycle.

#### 3.1.1. Bulk circulation flow phenomenon

Fig. 3 illustrates the flow direction for a full cycle for the methanol PHP at the heating power of 30.0 W. On the top of each subfigure, a solid or dashed arrow is drawn, with the solid line for the bulk circulation flow, the dashed line for the flow direction switch flow. PHP is operating in the bulk clockwise flow in Fig. 3a and n, and in the bulk anticlockwise flow in Fig. 3f. The bulk circulation flow lasts longer time, with  $ET = 0.456 \text{ s}$  for the bulk clockwise flow in Fig. 3a, and  $ET = 0.544 \text{ s}$  for the bulk anticlockwise flow in Fig. 3f. For the bulk circulation flow, any two neighboring capillary tubes always have the inverse flow direction. The bulk

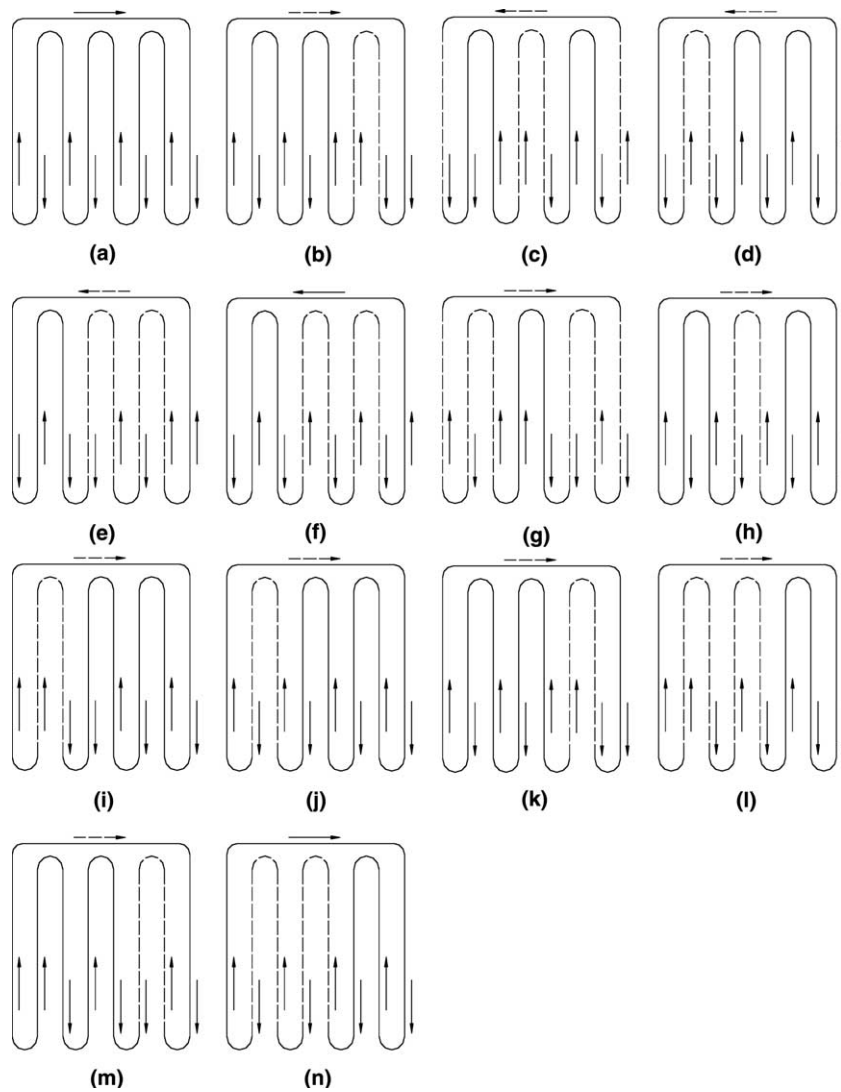


Fig. 3. Flow direction switch process in a full cycle ( $Q = 30.0$  W, methanol PHP). (a)  $ET = 0.456$  s, (b)  $ET = 0.104$  s, (c)  $ET = 0.052$  s, (d)  $ET = 0.104$  s, (e)  $ET = 0.08$  s, (f)  $ET = 0.544$  s, (g)  $ET = 0.056$  s, (h)  $ET = 0.048$  s, (i)  $ET = 0.08$  s, (j)  $ET = 0.16$  s, (k)  $ET = 0.064$  s, (l)  $ET = 0.04$  s, (m)  $ET = 0.016$  s and (n)  $ET = 0.16$  s.

circulation flow is similar for different heating powers and working fluids.

The bulk circulation flow is the major mechanism that transfers the heat from the evaporator to the condensation section. The process is similar to a convective two-phase flow system for which the evaporator section acts as the heat receiving part while the condensation section as the final heat sink. However the circulation flow is created automatically without mechanical moving components in the PHP system.

### 3.1.2. Local flow direction switch phenomenon

It is shown that when PHP is trying to switch one bulk circulation flow to another bulk circulation flow,

not all of the capillary tube changes the flow direction simultaneously. It is also found that for a specific capillary tube, the flow direction may be changed for several times for such bulk circulation flow switch, which is referred as the “local flow direction switch” phenomenon identified in the present paper.

The eight parallel capillary tubes are grouped as 1, 2, 3, each group consisting of two capillary tubes sharing the same inverted U bend in the condensation section, containing tubes from 2 to 7, as shown in Fig. 1b. The left and right side tubes are marked as 1 and 8 but not grouped.

The flow direction switch process from Fig. 3a to f is as follows: at first the capillary tubes for group 1 change

the flow direction, in which the tube II switches the upward flow in Fig. 3a to the downward flow in Fig. 3b, meanwhile the tube III switches the downward flow in Fig. 3a to the upward flow in Fig. 3b. In this process, all the other tubes sustain the same flow directions as shown in Fig. 3a. Thus in Fig. 3b both of the tubes I and II share the downward flow, while the tubes III and IV share the upward flow. Such flow transition in Fig. 3b totally lasts 0.104 s. Then PHP evolves into the flow transition in Fig. 3c. Both of the tubes IV and V of group 2 changes the flow direction. Such local flow direction switch process continues until the flow state shown in Fig. 3f is reached, possessing the bulk anti-clockwise circulation flow. PHP stays at this stage for 0.544 s. Then similar flow switch process is performed until the bulk clockwise circulation flow is reached shown in Fig. 3n. In the half cycle from Fig. 3g to n, the tubes of the group 1 totally changes the flow direction for 3 times, the group 2 tubes for 3 times, and the group 3 tubes for 5 times.

It is observed that during the local flow direction switch stage, some capillary tubes which share the U bend in the evaporator section may have the same flow direction. For instance, the tubes I and II share the downward flow shown in Fig. 3b, due to the compressible effect of the two-phase mixture in the evaporator section.

From one bulk circulation flow to another bulk circulation flow, any specific tube may change the flow direction for several times. The number of times that a specific tube changes the flow direction strongly depends on the heating powers. Lower heating powers lead to the less number of times for the flow direction switch process.

The local flow direction switch process could be caused by the combined effects of local boiling, condensation, bubble coalescence, etc. Such flow direction switch process will soon propagate to other locations, until all the flow directions in each tube are changed inversely to the initial bulk circulation flow.

### 3.2. Bubble displacement and velocity

We use the commercial software Photoshop 6 to analyze the bubble displacements and velocities. The data process involves the correlation of the bubble displacement versus time which is written as  $z = f(t)$ . Differentiating the bubble displacement against time yields the bubble velocity, i.e.,  $U(z) = dz/dt$ . Before doing so, the one-dimensional coordinate system should be established, which is attached on the vertical centerline of each capillary tube. If a bubble can cross the inverted U bend in the condensation section, the inverted U bend is stretched to be vertical. The original point of the coordinate axis is 3.5 mm higher than the maximum point of the centerline of the inverted U bend. Fig. 4a shows the

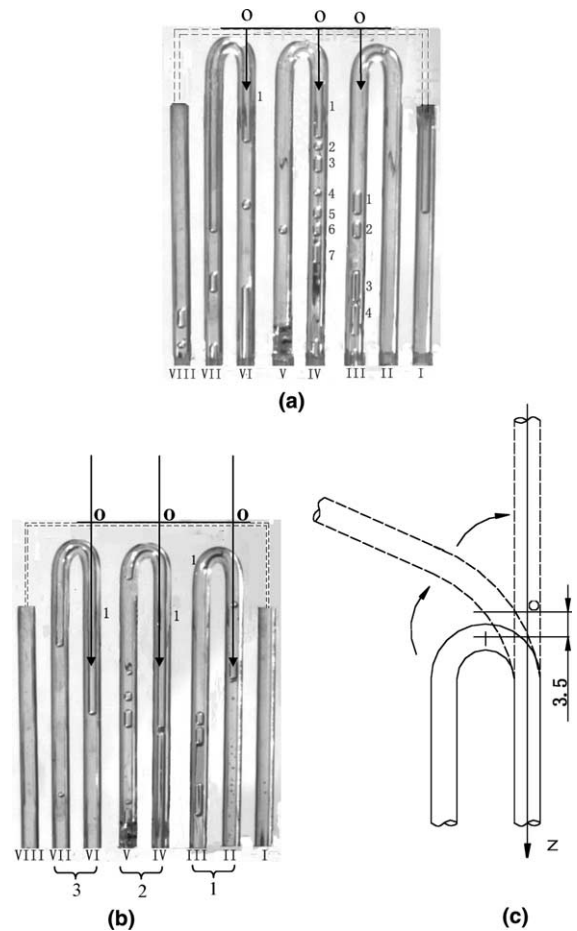


Fig. 4. Bubble images at specific times and stretched coordinate system for bubbles flowing across the inverted U bend, methanol PHP: (a)  $Q = 10.0$  W, (b)  $Q = 30.0$  W and (c) stretched coordinate system.

bubble image at the heating power of 10.0 W on a specific time, Fig. 4b for the heating power of 30.0 W, while the formation of the stretched coordinate system is shown in Fig. 4c.

Fig. 5 shows the bubble displacements and velocities at the heating power of 10.0 W (Fig. 5a) and 30.0 W (Fig. 5b) for the methanol PHP. The selected bubbles are named as “IV-1” and “II(III)-1”. “IV” is the number of the capillary tube while “1” is the selected bubble. “II(III)” is the number of the capillary tube while the bubble can cross the inverted U bend. It is seen that both of the bubble displacements and velocities are oscillating versus time as the quasi-sine oscillation waves, with the phase angle of  $90^\circ$  between them. However, some local oscillation waves in very short time periods with small amplitudes are superimposed with the sine oscillation wave for the bubble velocities, which are identified to be related to the local flow direction switch process as

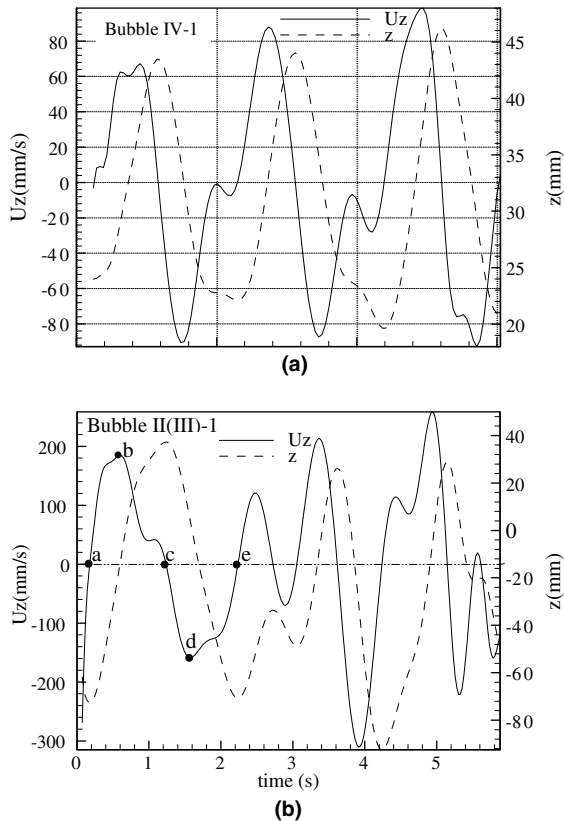


Fig. 5. Bubble displacements and velocities for the methanol PHP: (a)  $Q = 10.0$  W and (b)  $Q = 30.0$  W.

described in the “flow direction switch” section. The oscillation cycle period can be detected as the time from the neighboring maximum points, or the neighboring minimum points. The computed oscillation cycle period was 1.1 s and 2.2 s for the heating powers of 10.0 W and 30.0 W, respectively. Generally the sine oscillation waves for velocities are symmetrical about the centerline of  $U_z = 0$  at the lower heating powers.

Comparing Fig. 5a and b, it is concluded that at the lower heating power, the cycle period is shorter and the oscillating amplitude is smaller. The steady oscillation state can be easily reached. At the higher heating power such as 30.0 W, the oscillation cycle period is longer while the oscillation amplitude of the bubble displacement is larger. Severe local oscillation waves are superimposed with the quasi-sine oscillation waves. The PHP displays more random pulsating flow behavior, corresponding to the complicated local flow direction switch process described above.

The major parameters affecting the bubble velocities are the self-sustained pressure gradient, the bubble size and the buoyancy force. Over the same pressure gradient, small bubble size leads to large surface to volume ratio of the bubbles, causing the large buoyancy force

effect. Thus for the upward flow, smaller bubbles always have larger upward flow velocities, causing the smaller bubbles chasing the leading vapor plug. However, for the downward flow, smaller bubble sizes have slower downward velocities because the flow direction is inverse to the buoyancy force. The flow velocity differences among the different size bubbles are the major reason for the bubble coalescence.

PHP shows distinct characteristics if DI water is used as the working fluid. It is identified that in a full cycle for the water PHP, the fluid in the capillary tube stays at the quasi-stationary state for a longer time, at a specific time the fast movement of the fluid is suddenly initiated, then the PHP switches to the stationary state again. The PHP sustains the fast movement state only for a short time. PHP repeats the above “stationary–fast movement–stationary–fast movement” process cycle by cycle. However, in a full cycle, when the PHP is in the stationary state, some small amplitude oscillations are also identified.

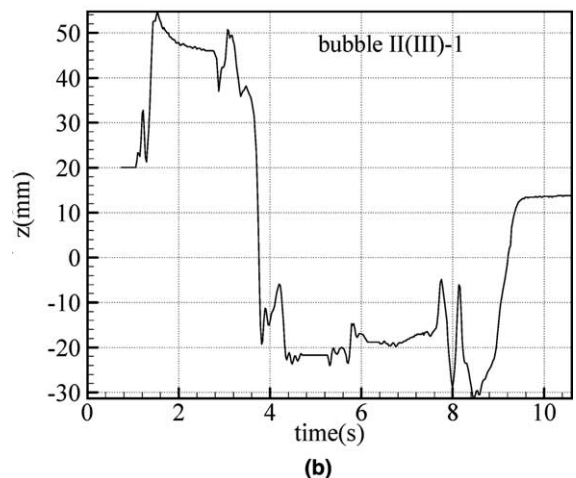
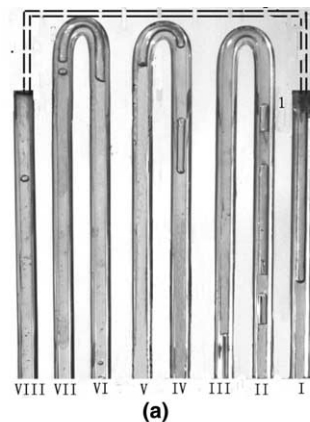


Fig. 6. Bubble images and the selected bubble displacements for the water PHP at the heating power of 30.0 W.

Fig. 6a and b show the bubble image for the water PHP at a specific time and the bubble displacement of the selected bubble “II(III)-1”, respectively. Because the quasi-rectangular bubble displacement curve is superimposed with random oscillation waves thus it is difficult to differentiate the curve versus time to obtain the bubble velocities. The bubble is nearly stationary in the period from 1.6 s to 3.6 s. At  $t = 3.6$  s a fast bubble movement is initiated, which only lasts 0.4 s with the displacement approaching 70 mm from  $t = 3.6$  s to 4.0 s. The mean velocity at this short period is estimated to be 180 mm/s. In the period of  $t = 4.0$ –8.4 s PHP returns to the quasi-stationary state. The time that the PHP is in the quasi-stationary state is much longer than that in the fast movement state.

The periodic movement behavior of the water PHP is possibly due to the large latent heat of evaporation. For the same heat received by water and methanol, less vapor volume and mass will be produced for water. Once the water PHP is in the movement state, heat can be transferred from the evaporator to the condensation section. However, such movement can only be sustained for a while, then the PHP would wait for sometime to accumulate enough “energy” thus the new movement can be activated.

## 4. Flow patterns

### 4.1. Flow pattern definition in PHP

Detailed flow patterns are reported using the high speed flow visualization system. Three types of flow patterns are characterized in terms of bubble sizes: dispersed bubbles, vapor plugs, and long vapor plugs. The water PHP has similar flow patterns except that the long vapor plugs do not exist. The bubble sizes are characterized as the diameter and the length. The flow patterns are shown in Fig. 7, in which *a, b, c* represent the dispersed bubbles, *f, g, h* for the vapor plugs, *i, j* for the long vapor plugs. It is noted that *d, e, f* indicate the

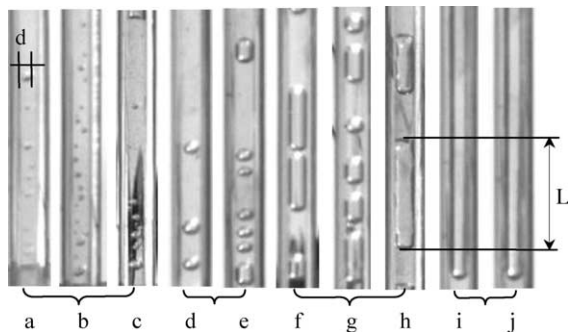


Fig. 7. Flow patterns taking place in PHP.

transition flow patterns from the dispersed bubbles to the vapor plugs, at which the bubble diameter approaches the inside diameter of the capillary tube.

#### 4.1.1. Dispersed bubbles

The diameter of the dispersed bubbles are less than the inside diameter of the capillary tube (see Fig. 7a–c). The dispersed bubbles are created by the continuous nucleated boiling if the coalescence does not occur in the evaporator section. The inside wall surface and the very fine particles dissolved in the liquid such as  $N_2$  are the nucleation cavities of the dispersed bubbles. The dispersed bubbles are so small that they are quickly condensed in the condensation section once they are out of the evaporator section. They may be fully condensed before they reach the top of the inverted U bend. It is also observed that the dispersed bubbles may collide the inside wall surface of the capillary tube, but may return to the core flow and continue the upward flowing toward the top of the inverted U bend.

A lot of parameters affect the nucleation boiling process in the evaporator section, such as the number of capillary tubes, the height of the PHP, the inside diameter of the capillary tube, the bond number,  $Bo = g(\rho_f - \rho_g)D^2/\sigma$ . Among them  $Bo$  number should be the most important parameter governing the boiling process, in terms of the available boiling heat transfer studies in macroscale. If  $Bo$  is larger than a critical value, the system will no longer be a pulsating heat pipe. The working fluid will settle down by gravity and the device will function either as a gravity assisted thermosyphon, or as an interconnected array of the phase change gravity assisted thermosyphon, with pool boiling heat transfer controlling the performance. Therefore the different heat flux and the charging ratio not only influence the flow patterns, but also the different heat transfer mechanisms [8].

Very low heat flux may lead to the “nucleate pool boiling” or “free convection nucleate boiling”. Increasing heat flux evolves the nucleate boiling. In this region, the thermal performance in the evaporator section mainly relied on the heat flux, not on the self-sustained flow velocity. However, on the very high heat flux range, the PHP performance will mainly depends on the self-sustained flow velocity, less dependent on the heat flux. The self-sustained flow velocities satisfy the quasi-sine oscillation waves, as described previously, at least for the methanol PHP.

The dispersed bubbles have the large possibilities that exist in the vertical upward flow. When the flow direction is changed from the downward to the upward flow for a specific tube, the dispersed bubbles can be observed. These dispersed bubbles are coming from the evaporator section. They may be fully condensed before they reach the top of the inverted U bend thus there are less dispersed bubbles sustaining the downward flow in

the neighboring tube. This is the major reason why there are less dispersed bubbles in the vertical downward flow. On the other hand, once a specific tube establishes the downward flow, the dispersed bubbles created in the evaporator section are pushed downward by the pressure gradient thus they are not observed in such tube.

#### 4.1.2. Transition flow patterns from the dispersed bubbles to the vapor plugs

It is observed that the spherical bubbles have the sizes approaching the inside diameter of the capillary tube, providing a size link from the dispersed bubbles to the vapor plugs (see Fig. 7d–e). These bubbles are coming from the following mechanisms: dispersed bubble coalescence, vapor plug condensation (the vapor plug can be shortened by condensation heat transfer to become the transition bubble size), long vapor plug breakup for the water PHP, which will be analyzed in a separate section.

#### 4.1.3. Vapor plug and long vapor plugs

Vapor plugs have the diameter approaching the inside diameter of the capillary tube, but have the length larger than the diameter of the inside tube (see Fig. 7f–h). There are no much differences for the vapor plug flow in the capillary tubes of PHP and the macrochannels [10,11]. There is a liquid bridge between two neighboring vapor plugs. A thin liquid film separates the vapor core and the inside wall surface, with the inverse flow direction to the vapor core flow. This is true for both upward and downward flow, satisfying the fluid mechanics requirements of the standard slug flow [10]. The methanol PHP is observed to have the symmetry end shapes with the nearly same advancing and receding interface curvatures. However, the water PHP has the protruding advancing interface but has the flat receding interface for the vapor plug flow. The advancing and receding interface difference among the two different working fluids are due to the surface tension effects. Water has larger surface tension than that of methanol.

Very long vapor plugs were also observed for methanol PHP (see Fig. 7i–j), but not observed for the water PHP, due to the vapor plug breakup mechanism.

#### 4.2. Time and space dependent bubble size distributions

Partially charging the liquid in the capillary tube results in the randomly distributed vapor plug trains. The two-phase structure will be collapsed once heating is applied over the PHP system, but the new bubble size distribution will be created. The integrated bubble numbers were plotted versus the bubble sizes at five different specific times in Fig. 8a–f for the methanol PHP at the heating power of 30.0 W, in which a–f are corresponding to the time at which the bubbles have the velocities of zero, maximum, zero, minimum, and zero in a full cycle

(see Fig. 5b). These five time segments represent the five specific velocity characteristics. The full picture of the time dependent bubble size distributions can not be identified using too less time segments. On the other hand, it is not necessary to use more time segments than five because PHP shows the periodic oscillation behavior. It is seen from Fig. 8 that: (1) Three types of bubbles coexist in PHP including the transition flow patterns with the bubble size approaching the inside diameter of the capillary tube. (2) The bubble size distributions are almost similar at different time in a full cycle. (3) The total numbers of dispersed bubbles, vapor plugs and long vapor plugs are nearly constant at different time in a full cycle. However, the numbers of the dispersed bubbles are varied from time to time, but have less influence on the overall vapor volume over the entire PHP system.

Similar conclusions can be drawn for the water PHP. As stated earlier, the water PHP does not have the long vapor plugs.

Fig. 8g illustrates the bubble size distributions between different tubes over two oscillation cycles. It is interesting to note that the bubble sizes have an unsymmetry distribution between the different tubes. The numbers of the dispersed bubbles are great in the right side tubes (tubes 1 and 2). Generally all of the bubble sizes within the range of 1 to more than 100 mm have distributions for each capillary tube. However, the bubble numbers for each bubble size are gradually decreased from tube 1 to 8. In each capillary tube, bubbles have largest distributions around the bubble length of 5 mm, 2.5 times of the inside diameter of the capillary tube. A lot of parameters influence the bubble size distributions: the uniformity of the heat flux applied on the evaporator section, bubble nucleation, coalescence and condensation. However, in the author's opinion, the initial unsymmetry bubble size distribution before heat is received by PHP is responsible for the unsymmetry bubble size distribution in the PHP operation state.

#### 4.3. Bubble coalescence and condensation

Bubble coalescence takes place for any working fluid and heating power, reflecting the bubble interaction mechanism, which has three characteristics: (1) The distance between two neighboring bubbles are short. (2) The two neighboring bubbles have different lengths. (3) For the vertical upflow, the leading bubble is always longer than the trailing bubble which has larger velocity. However, for the vertical downflow, the leading bubble is shorter than the trailing bubble which has larger velocity. Fig. 9a illustrates the time advancing series of the bubble coalescence. With time advancing the trailing vapor plug (bubble B) is chasing the leading vapor plug (bubble A) so that bubble coalescence can take place. The bubble coalescence mechanism can be analyzed

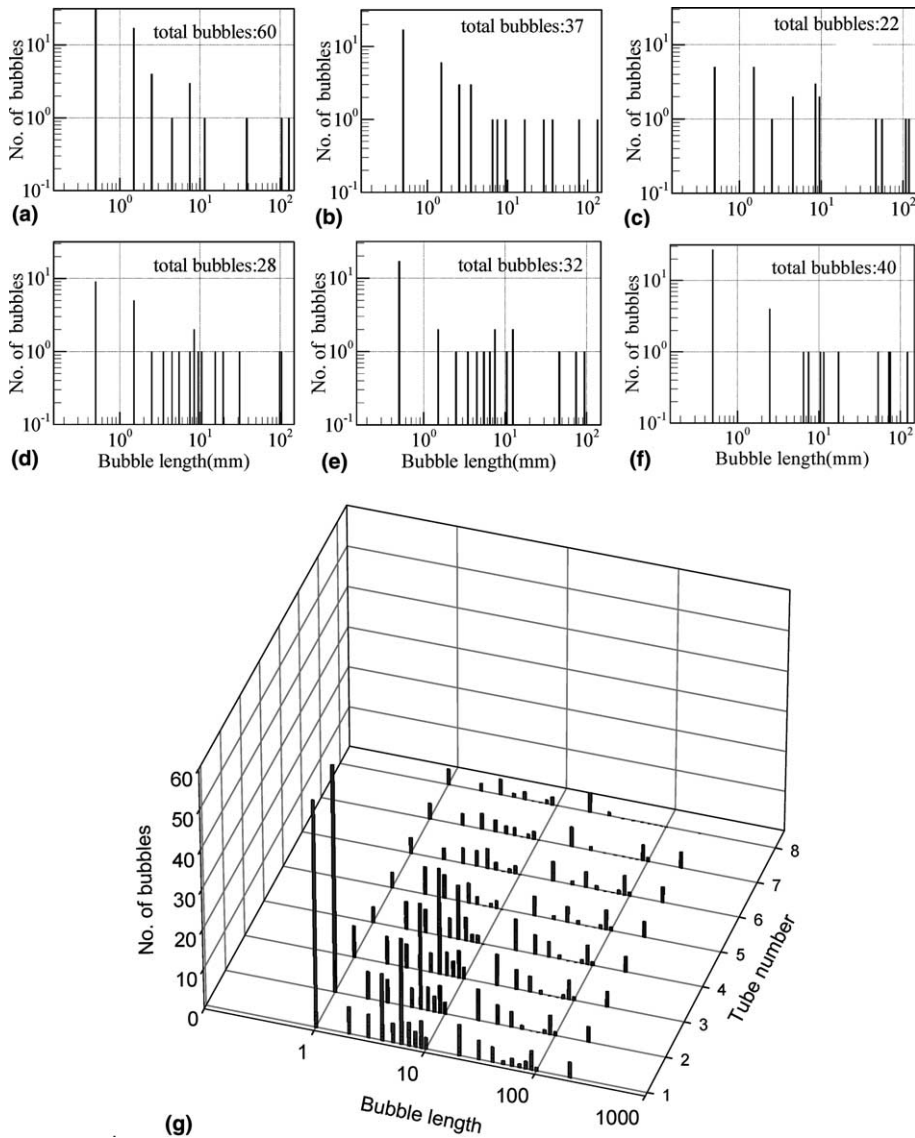


Fig. 8. Time and space dependent bubble size distributions for the methanol PHP at the heating power of 30.0 W.

using the available slug flow theory developed for macrochannels [12]. Assuming a vapor plug is leading a dispersed bubble or a vapor plug with shorter length. The two bubbles have a short liquid bridge between them. A thin liquid film with the downward flow direction which is inverse to the vapor core is surrounding the leading vapor plug. The downward liquid film flow results in a higher upward velocity of the liquid bridge, causing the faster pumping effect of the trailing bubble. With time evolving the two bubbles are mixed. Such explanation is also valid for the vertical downflow.

Bubbles always have higher temperatures than the inside wall surface of the capillary tube in the condensation section thus bubble condensation occurs. As

shown in Fig. 9b, bubbles A–C have the decreased lengths versus time until they are totally disappeared. Dispersed bubbles could be condensed in the liquid core therefore there is an indirect heat transfer between the dispersed bubbles and the tube wall. Vapor plugs formed by the bubble coalescence induces the direct condensation heat transfer between the vapor core and the tube wall thus heat transfer from the PHP system to the environment is enhanced, while condensation heat transfer is a common mode for the heat transfer process in PHP.

In the evaporator section, bubble nucleation and coalescence causes the local void fraction to change with respect to time. Bubble nucleation induces the increased

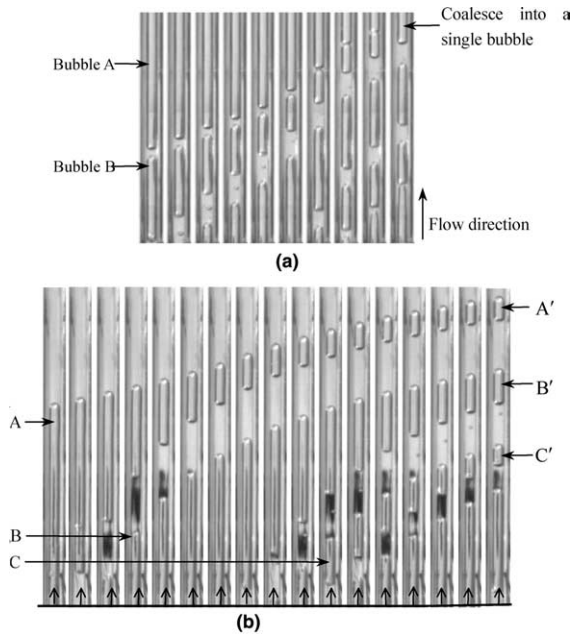


Fig. 9. Time series of bubble coalescence and condensation for the methanol PHP at the heating power of 30.0 W: (a)  $\Delta t = 0.016$  s,  $\Delta T = 0.144$  s and (b)  $\Delta t = 0.016$  s,  $\Delta T = 0.256$  s.

number of vapor bubbles whereas bubble coalescence causes the decreased numbers of vapor bubbles. When the local wall surface is temporarily occupied by the vapor plug, the continuous heating may result in the local dry-out. Once such local wall surface is flushed by the incoming liquid slug, the nucleation boiling could be initiated again. The vapor plug and liquid slug distributions are important to trigger the nucleation boiling in the evaporator section.

Local oscillations could be due to the combined effects of bubble nucleation, coalescence and condensation. These processes occur at different locations of the PHP tubes and the local disturbance will be propagated through the vapor plug train units to other PHP locations. The propagation of disturbance can be complex because the vapor plugs and liquid slugs are randomly distributed. Future numerical modeling should be performed for the PHP bubble dynamics.

#### 4.4. Vapor plug deformation and breakup

It is observed that when the vapor plug is traveling in the capillary tubes of the water PHP, the advancing and receding angles are different, due to the large surface tension of the working fluid. Besides, the water PHP has the periodic “stationary–fast movement” behavior. When the vapor plug is suddenly in the stationary state, the pressure drop over the two ends of the vapor plug

becomes zero. However, the unsymmetry end shapes of the advancing and receding vapor–liquid interfaces is not changed, causing the liquid accumulated in specific regions. Further expansion of the liquid lobe will finally breakup the vapor plug. Fig. 10 shows the time series of the vapor plug breakup process in the inverted U bend region. It is observed that when the vapor plug was traveling in the capillary tube with anticlockwise direction before its stationary state, the liquid lobe forms on the outer bending tube (see Fig. 10a). However, the clockwise flow direction before its stationary state results in the liquid lobe formation in the inner bend tube (see Fig. 10b).

There are some non-dimensional parameters governing the two-phase flow in the capillary tubes in which surface tension effect is significant. The bond number is defined as  $Bo = g(\rho_f - \rho_g)D^2/\sigma$ , indicating the ratio of the buoyancy force to the surface tension force, with the inside diameter of the capillary tube,  $D$ , as the characteristic length. The  $EO$  number is similar to the bond number except that the characteristic dimension  $L$  could be any other physically relevant parameter. They are identical when  $L$  is set as  $D$ . The capillary number is defined as  $Ca = \mu U/\sigma$ , representing the ratio of viscous to surface tension forces. Other parameters, such as the boiling number ( $Bo^*$ ), Weber number ( $We$ ) may not be related to the present problem analysis, thus they are not written here but could be found in Kandlikar [13]. For the present vapor plug deformation and breakup process, The  $Bo$  and  $Ca$  numbers are the important scaling parameters, involving the gravity forces of the two-phases, the buoyancy force and the viscous force. Recently Allen and coworker [14] reported that for the capillary pumping loop (CPL) operating at the low gravity environment on board the Space Shuttle Columbia in July of 1997, an interesting phenomenon was observed that liquid would accumulate in the curved portion and suddenly transition into a liquid slug and terminate the fluid circulation. Allen and coworker [14] gave a detailed literature review and proposed a model describing the process.

The schematic mechanism of the liquid lobe formation is shown in Fig. 11, in which  $R_i$  is the inside radius of the capillary tube,  $h$  is the thickness of the liquid film,  $R_b$  is the centerline curvature radius of the inverted U bend. Six distinct liquid regions are illustrated in Fig. 11. The first region 1 is the right-top corner relative to the concave interface in the inverted U bending tube. Region 2 is the right-lower corner referring to the concave interface. Region 3 is the outer side of the bending tube where the liquid accumulates. Region 4 is the inside of the bending tube and is located  $180^\circ$  from region 3. Region 5 is the circumference liquid film separating the vapor core and the inside wall surface. Region 6 is the liquid adjacent to the protruding vapor–liquid interface in the straight tube. Because the inside diameter of

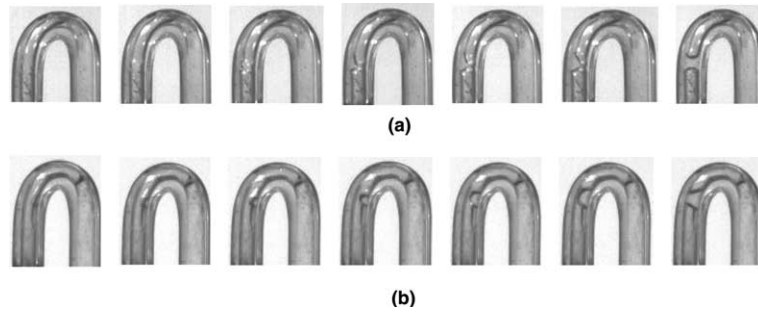


Fig. 10. Time series of vapor plug deformation and breakup process in the bending tube: (a) anticlockwise flow before its stationary state,  $\Delta t = 0.024$  s,  $\Delta T = 0.144$  s; and (b) clockwise flow before its stationary state,  $\Delta t = 0.048$  s,  $\Delta T = 0.288$  s.

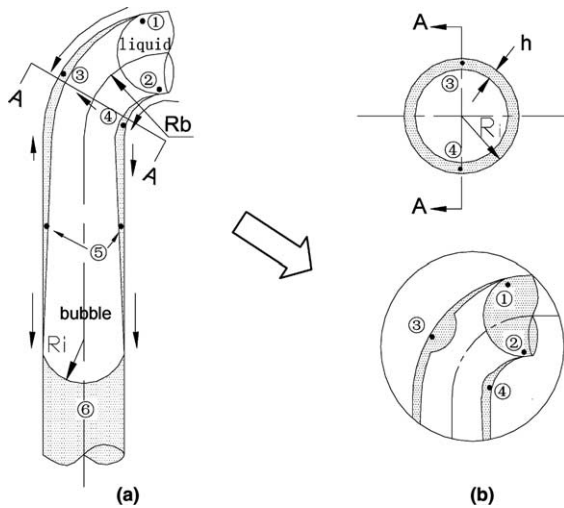


Fig. 11. Vapor plug deformation and breakup mechanism for the anticlockwise flow before its stationary state.

the capillary tube is small, the water PHP system belongs to the low bond number system.

Liquid will be accumulated in regions 3 and 4 to form the liquid lobe (see Fig. 11). Such liquid accumulation process is dominated by the capillary pressure difference between each of regions. For any vapor–liquid interface, the Laplace–Young equation is written as

$$p_v - p_l = \sigma \left( \frac{1}{R_1} + \frac{1}{R_2} \right), \tag{1}$$

where  $p_v$  is the vapor pressure and  $p_l$  is the liquid pressure.  $R_1$  and  $R_2$  are the principal radius of the curvatures. One of the principal radius is the same for all the regions and is equal to  $\pm(R_i - h)$ . The negative sign is for regions 1 and 2, positive sign is for other regions. The other radius is different from region to region. For region 1 such radius of the curvature is  $-(R_i - h)$ . The second principal radius for regions 2–6 are  $-(R_i - h)$ ,  $[R_b + (R_i - h)]$ ,  $-[R_b - (R_i - h)]$ ,  $\infty$ ,  $R_i - h$ , respectively. Table 1 listed the radius for each region and the corresponding values for the present PHP, in which  $R_b = 6$  mm,  $R_i = 1$  mm. It is difficult to decide the liquid film thickness,  $h$ . For the present problem analysis, the liquid film thickness of 500  $\mu$ m is used. The sensitivity analysis shows that when  $h$  varied from 0.02 mm to 0.07 mm, the flow direction and the relative flow rate magnitude between each of liquid regions are not changed. It is noted that Allen and coworker [14] used  $h$  of 350  $\mu$ m for the liquid lobe formation analysis.

The unit form is the real value, while the deformed form is still in unit but using the non-dimensional liquid film thickness  $\delta$  and the non-dimensional radius ratio  $\Gamma$ , which are defined as

$$\delta = \frac{h}{R_i}, \quad \Gamma = \frac{(R_i - h)}{R_b}. \tag{2}$$

Table 1  
Curvature radius for the six regions corresponding to Fig. 11

| Region | Curvature radius |                    |                      |  | Values for deformed form |            |
|--------|------------------|--------------------|----------------------|--|--------------------------|------------|
|        | $R_1$            |                    | $R_2$                |  | $R_1$ (mm)               | $R_2$ (mm) |
|        | Unit form        | Deformed form      | Unit                 | Deformed form  |                          |            |
| 1      | $-(R_i - h)$     | $-R_i(1 - \delta)$ | $-(R_i - h)$         | $-R_i(1 - \delta)$                                     | −0.95                    | −0.95      |
| 2      | $-(R_i - h)$     | $-R_i(1 - \delta)$ | $-(R_i - h)$         | $-R_i(1 - \delta)$                                     | −0.95                    | −0.95      |
| 3      | $R_i - h$        | $R_i(1 - \delta)$  | $[R_b + (R_i - h)]$  | $R_i(1 - \delta) \frac{1+\Gamma}{\Gamma}$              | 0.95                     | 6.95       |
| 4      | $R_i - h$        | $R_i(1 - \delta)$  | $-[R_b - (R_i - h)]$ | $R_i(1 - \delta) \left(\frac{\Gamma-1}{\Gamma}\right)$ | 0.95                     | −5.05      |
| 5      | $R_i - h$        | $R_i(1 - \delta)$  | $\infty$             | $\infty$   | 0.95                     | $\infty$   |
| 6      | $R_i - h$        | $R_i(1 - \delta)$  | $R_i - h$            | $R_i(1 - \delta)$                                      | 0.95                     | 0.95       |

Assuming an uniform pressure inside the vapor core, using the two principal radius listed in Table 1 and substituting Eq. (2) into Eq. (1) obtains

$$\left. \begin{aligned} \Delta p_{f,1-3} &= \frac{\sigma}{R_i(1-\delta)} \frac{3+4\Gamma}{1+\Gamma} \\ \Delta p_{f,2-4} &= \frac{\sigma}{R_i(1-\delta)} \frac{3-4\Gamma}{1-\Gamma} \\ \Delta p_{f,5-3} &= \frac{\sigma}{R_i(1-\delta)} \frac{\Gamma}{1+\Gamma} \\ \Delta p_{f,4-5} &= \frac{\sigma}{R_i(1-\delta)} \frac{\Gamma}{1-\Gamma} \\ \Delta p_{f,5-6} &= \frac{\sigma}{R_i(1-\delta)} \\ \Delta p_{f,4-3} &= \frac{2\sigma}{R_i(1-\delta)} \frac{\Gamma}{1-\Gamma^2} \end{aligned} \right\} \quad (3)$$

$\Delta p_{f,i-j}$  is the pressure difference from region  $i$  to  $j$ . Eq. (3) describes the pressure difference resulted from the capillary effect between each of the six liquid regions shown in Fig. 11. If the liquid film is stable and mainly dominated by the viscous force, the governing equations can be reduced to the lubrication approximation. For  $\delta \sim 1$ , the velocity in the liquid film can be scaled as

$$U \sim \frac{\delta R_i}{\mu} \frac{\Delta p_f}{L} \quad (4)$$

where  $\mu$  is the liquid viscosity,  $L$  is the characteristic length over which the pressure difference takes place. Eq. (4) is only correct if both  $\delta \ll 1$  and  $\Gamma \ll 1$  are satisfied. If  $\Gamma$  approaches 1, the bend radius approaches the inside radius of the capillary tube. The curvature effects associated with  $R_b$  becomes important and can not be neglected. For the present PHP,  $\Gamma = 1/6$ . The characteristic length  $L$  from regions 4 to 3 associated with the pressure difference,  $\Delta p_{f,4-3}$ , is the half of the perimeter of the inside tube,  $\pi R_i$ . From regions 1 to 3, and from regions 2 to 4, associated with the pressure differences,  $\Delta p_{f,1-3}$  and  $\Delta p_{f,2-4}$ , the characteristic lengths are the half of the outer arc and the inner arc of the bending tube. Between regions 5 and 3, and between regions 5 and 4, the length scale is the arc length from the bend to the straight section.

The liquid flow between each of liquid regions can also be rewritten using the capillary number, scaling the viscous force over the capillary force. The capillary number is defined as

$$Ca = \frac{\mu U}{\sigma} \quad (5)$$

The capillary number between each of the six liquid regions can be obtained using the pressure difference expression,  $\Delta p_f$ , the characteristic length associated with the corresponding pressure difference, and the velocity scale in the liquid film. The resulted capillary numbers between each of the regions are as follows:

Table 2  
Capillary numbers between each of liquid regions corresponding to Fig. 11

| Regions          | 1-3 | 2-4 | 5-3  | 4-5  | 5-6 | 4-3 |
|------------------|-----|-----|------|------|-----|-----|
| $Ca \times 10^5$ | 553 | 496 | 3.29 | 6.24 | 176 | 28  |

$$\left. \begin{aligned} Ca_{1-3} &\sim \frac{2}{\pi} \left[ \frac{\delta}{1-\delta} \right]^2 \frac{3+4\Gamma}{1+\Gamma} \\ Ca_{2-4} &\sim \frac{2}{\pi} \left[ \frac{\delta}{1-\delta} \right]^2 \frac{3-4\Gamma}{1-\Gamma} \\ Ca_{5-3} &\sim \frac{2}{\pi} \left[ \frac{\delta}{1-\delta} \right]^2 \left[ \frac{\Gamma}{1+\Gamma} \right]^2 \\ Ca_{4-5} &\sim \frac{2}{\pi} \left[ \frac{\delta}{1-\delta} \right]^2 \left[ \frac{\Gamma}{1-\Gamma} \right]^2 \\ Ca_{5-6} &\sim \frac{2}{\pi} \left[ \frac{\delta}{1-\delta} \right]^2 \\ Ca_{4-3} &\sim \frac{2}{\pi} \left[ \frac{\delta}{1-\delta} \right]^2 \frac{\Gamma}{1-\Gamma^2} \end{aligned} \right\} \quad (6)$$

The final capillary numbers between each of regions are found to be depended upon  $\delta$  and  $\Gamma$ . They are not influenced by the working fluids. Substituting the corresponding values into Eq. (6), we attain the capillary numbers as shown in Table 2.

If computed  $Ca_{i-j} > 0$ , the liquid flow will be initiated from regions  $i$  to  $j$ . The magnitude of  $Ca$  number scales the liquid flow rate between each of regions. Fig. 11a shows the flow direction between each of regions. The arrow represents the flow direction and the length of the arrow reflects the flow rate, qualitatively. Liquid is accumulated in region 3. Also the net liquid flow rate toward region 4 is positive thus liquid is also accumulated in region 4. However, liquid accumulated in region 3 is more than that in region 4. Fig. 11b is the enlarged vapor plug configuration. With time evolving more and more liquid is accumulating in region 3 and the vapor plug is broken up. The present theoretical analysis gives a good explanation of the vapor plug breakup process.

### 5. Conclusions

The following conclusions can be drawn based on the present high speed flow visualization of the closed loop pulsating heat pipe.

1. In a full cycle, there exists bulk circulation flow and local flow direction switch flow. Bulk circulation flow sustains longer while the local flow direction switch flow shorter. From one bulk circulation flow to the inverse bulk circulation flow, the local flow direction switch flow occurs for a group of tubes sharing the same inverted U bend in the condensation section,

alternatively. For a specific tube, flow direction may be changed for several times for such bulk flow transition.

2. The methanol PHP does behave the quasi-sine oscillating wave for bubble displacements and velocities. The cycle periods and the oscillating amplitudes are increased with increasing the heating powers. Higher heating powers result in more severe local random oscillating nature with short time periods and small amplitudes superimposed, due to the complicated local flow direction switch process. The water PHP displays the periodic “stationary–fast movement” behavior due to its large evaporation of heat. The bubble displacement versus time has quasi-rectangular shape.
3. There exist dispersed bubbles, vapor plugs and transition flow patterns in PHP. Long vapor plugs are only observed in the methanol PHP, not observed in the water PHP. The bubble sizes have quasi-stable distributions versus time over the entire PHP system. However, the unsymmetry bubble size distributions among the different tubes are identified, related to their initial random bubble size distributions.
4. The bulk circulation flow and the local flow direction switch flow are induced by the combined effects of bubble nucleation, coalescence and condensation.
5. A theoretical model was used to explain the vapor plug deformation and breakup process occurred in the water PHP. The vapor plugs have different advancing and receding vapor–liquid interfaces. Once such vapor plug is in the stationary state, the non-uniform capillary pressures between each of the liquid regions are responsible for the liquid accumulated in some specific regions, leading to the vapor plug deformation and breakup process.

### Acknowledgement

This work is supported by the Natural Science Foundation of China (50476088), Natural Science Foundation of Guangdong Province (32700) and the Science and Technology Development Foundation of Guangdong Province (33103).

### References

- [1] H. Akachi, Structure of a heat pipe, 1990, U.S. Patent 4921041.
- [2] K. Gi, S. Maezawa, Y. Kojima, N. Yamazaki, CPU cooling of notebook PC by oscillating heat pipe, in: Proceedings of 11th International Heat Pipe Conference, Tokyo, Japan, 1999, pp. 166–169.
- [3] T.N. Wong, B.Y. Tong, S.M. Lim, K.T. Ooi, Theoretical modeling of pulsating heat pipe, in: Proceedings of 11th International Heat Pipe Conference, Tokyo, Japan, 1999, pp. 159–163.
- [4] M.B. Shafii, A. Faghri, Y.W. Zhang, Thermal modeling of unlooped and looped pulsating heat pipes, ASME, J. Heat Transfer 123 (2001) 1159–1172.
- [5] M.B. Shafii, A. Faghri, Y.W. Zhang, Analysis of heat transfer in unlooped and looped pulsating heat pipes, Int. J. Num. Meth. Heat Fluid Flow 12 (5) (2002) 589–609.
- [6] B.Y. Tong, T.N. Wong, K.T. Ooi, Closed-loop pulsating heat pipe, Appl. Therm. Eng. 21 (2001) 1845–1862.
- [7] P. Charoensawan, S. Khandekar, M. Schneider, M. Groll, Closed loop pulsating heat pipes. Part A: Parametric experimental investigations, Appl. Therm. Eng. 23 (2003) 2009–2020.
- [8] P. Charoensawan, S. Khandekar, M. Schneider, M. Groll, Closed loop pulsating heat pipes. Part B: Visualization and semi-empirical modeling, Appl. Therm. Eng. 23 (2003) 2021–2033.
- [9] X.M. Zhang, J.L. Xu, Z.Q. Zhou, Experimental study of a pulsating heat pipe using FC-72, ethanol, and water as working fluids, Exp. Heat Transfer 17 (2004) 47–67.
- [10] L. Shemer, Hydrodynamic and statistical parameters of slug flow, Int. J. Heat Fluid Flow 24 (2003) 334–344.
- [11] Q. Liao, T.S. Zhao, Modeling of Taylor bubble rising in a vertical mini noncircular channel filled with a stagnant liquid, Int. J. Multiphase Flow 29 (2003) 411–434.
- [12] E.T. Tudose, M. Kawaji, Experimental investigation of Taylor bubble acceleration mechanism in slug flow, Chem. Eng. Sci. 54 (1999) 5761–5775.
- [13] S.G. Kandlikar, Heat transfer mechanisms during flow boiling in microchannels, ASME J. Heat Transfer 126 (2004) 8–16.
- [14] J.S. Allen, K. Hallinan, Liquid blockage of vapor transport lines in low Bond number systems due to capillary driven flows in condensed annular films, Int. J. Heat Mass Transfer 44 (2001) 3931–3940.